AIP Journal of Applied Physics

Photoluminescence in disordered Sm-doped Pb Ti O 3 : Experimental and theoretical approach

R. C. Lima, J. W. M. Espinosa, M. F. C. Gurgel, E. C. Paris, E. R. Leite, M. R. Joya, P. S. Pizani, J. A. Varela, and E. Longo

Citation: Journal of Applied Physics **100**, 034917 (2006); doi: 10.1063/1.2230122
View online: http://dx.doi.org/10.1063/1.2230122
View Table of Contents: http://scitation.aip.org/content/aip/journal/jap/100/3?ver=pdfcov
Published by the AIP Publishing

Photoluminescence in disordered Sm-doped $PbTiO_3$: Experimental and theoretical approach

R. C. Lima[a)]
Departamento de Química, Universidade Federal de São Carlos, São Carlos, São Paulo 13565-905, Brazil

J. W. M. Espinosa
CCEN, Departamento de Química, Universidade Federal da Paraíba, Campus I, Cidade Universitária, João Pessoa, Paraíba 58059-900, Brazil

M. F. C. Gurgel, E. C. Paris, and E. R. Leite
Departamento de Química, Universidade Federal de São Carlos, São Carlos, São Paulo 13565-905, Brazil

M. R. Joya and P. S. Pizani
Departamento de Física, Universidade Federal de São Carlos, São Carlos, São Paulo 13565-905, Brazil

J. A. Varela and E. Longo
Instituto de Química, Universidade Estadual Paulista, Araraquara, São Paulo 14801-907, Brazil

(Received 17 March 2006; accepted 16 June 2006; published online 14 August 2006)

Sm-doped $PbTiO_3$ powder was synthesized by the polymeric precursor method, and was heat treated at different temperatures. The x-ray diffraction, photoluminescence, and UV-visible were used as a probe for the structural order degree short-, intermediate-, and long-range orders. Sm^{3+} ions were used as markers of these order-disorder transformations in the $PbTiO_3$ system. From the Rietveld refinement of the Sm-doped $PbTiO_3$ x-ray diffraction data, structural models were obtained and analyzed by periodic *ab initio* quantum mechanical calculations using the CRYSTAL 98 package within the framework of density functional theory at the B3LYP level. This program can yield important information regarding the structural and electronic properties of crystalline and disordered structures. The experimental and theoretical results indicate the presence of the localized states in the band gap, due to the symmetry break, which is responsible for visible photoluminescence at room temperature in the disordered structure. © *2006 American Institute of Physics*.
[DOI: 10.1063/1.2230122]

I. INTRODUCTION

The luminescence of different kinds of compounds has been extensively studied in doped crystalline samples or single crystals, due to their potential optoelectronic applications.[1–5] Semiconductors of titanate-type compounds ($ATiO_3$ where A=Pb, Ca, Sr, and Ba) have presented luminescence phenomena.[6–8] Myhajlenko *et al.*[9] investigated the optoelectronic characteristics of bulk single-crystal $SrTiO_3$ (STO) and epitaxial STO on Si by photoluminescence and cathodoluminescence techniques. These authors observed a qualitative correlation in the room temperature near-band-edge luminescence properties and crystalline quality using-micro-Raman spectroscopy and transmission electron microscopy. Chen *et al.*[10] investigated by cathodoluminescence at room temperature of the Al-doped single-crystalline $Ba_{0.6}Sr_{0.4}TiO_3$ thin films obtained by pulsed laser. The cathodoluminescence was related to the electronic transitions. Lin *et al.*[11] reported photoluminescence properties of nanosized $Na_{0.5}Bi_{0.5}TiO_3$ powder synthesized by a sol-gel process and observed that a self-trapped excitation might be responsible for the visible emission band. Hara[12] defined the electron-detrapping mechanism from localized states in the band gap of $(Ba,Sr)TiO_3$ films.

Due to their high technological interest, perovskite titanates are also the focus of numerous theoretical-computational studies. Often based on *ab initio* calculations, they can provide important information regarding the electronic and structural properties of solids and the interpretation of experimental data.[13–15]

Our group have performed theoretical and experimental studies, in particular, of $SrTiO_3$, $BaTiO_3$, and $PbTiO_3$ (PT) perovskites in disordered (noncrystalline) and ordered (crystalline) states.[16,17] Experimental results obtained by x-ray absorption near edge structure (XANES) for the structurally disordered phase revealed the coexistence of two types of Ti coordination in the PT,[16,18] namely, fivefold oxygen Ti coordination $[TiO_5]$ and sixfold oxygen Ti coordination $[TiO_6]$. We have also observed that $[TiO_5]$ is absent in well-crystallized titanates. Based on these experimental results, De Lazaro *et al.*[19] have modeled the PT structurally disordered by shifting Ti by a $(0,0,0.5)$ Å vector from its previous position in the former $1\times1\times2$ supercell. This Ti displacement represents the two experimentally detected environments of Ti, $[TiO_5]$ square-base pyramid, and $[TiO_6]$ octahedron. The theoretical results indicated the appearance of energy levels in the band gap. This is ascribed to a breakage in symmetry, which is responsible for visible photoluminescence in the disordered state material at room tempera-

a)Electronic mail: renata@liec.ufscar.br

ture. In addition, the polarity variation by Sm^{3+} introduction in the PT structure plays a significant role in the determining order-disorder of the PT.

There are numerous papers reporting Sm-doped materials. Zhang *et al.*[20] reported damage accumulation and amorphization in Sm titanate pyrochlore based on a disorder accumulation model that indicates a predominant role of a defect-stimulated amorphization process. Kodaira *et al.*[21] observed the photoluminescence behavior of the Sm^{3+} and Tb^{3+} ions doped into the $Gd_2(WO_4)_3$ matrix prepared by the Pechini and ceramic methods and observed that these tungstates present an intense luminescence emission. Singh *et al.*[22,23] measured dielectric, piezoelectric, and dilatrometric properties of Sm modified PCT ceramics and observed that both, tetragonality and relative density decrease with Sm substitution.

The substitution of a trivalent rare earth element (Sm^{3+}) into sites normally occupied by a divalent lead ion (Pb^{2+}) requires the presence of a compensating negative charge somewhere in the $PbTiO_3$ lattice. Achieving charge balance by means of lead vacancies can be effectively ruled out because one lead vacancy would compensate the charge of two samarium ions, according to the following equation:

$$Sm_2(TiO_3)_3 \xrightarrow{PbTiO_3} 2Sm^{\cdot}_{Pb} + V''_{Pb} + Ti^{x}_{Ti} + 9O^{x}_{o}. \qquad (1)$$

When rare earth ions with optical activity are added to perovskite-type structures it brings the possibility of studies of the ceramic class as luminescent materials of high performance. Rare earth doped silica glasses, ZrO_2, and other compounds for photonic applications, such as in optical amplification and optical devices, have also been extensively studied.[24–26] The Sm^{3+} rare earth ion is characterized by narrow bands in the photoluminescence spectrum.[27] This ion can be used as marker of the structural order-disorder in the materials.

In the present work, Sm^{3+} ions were added to a $PbTiO_3$ (PT:Sm) lattice via soft chemical synthesis—the so-called polymeric precursor method to investigate the order-disorder changes promoted by controlled heat treatments. The x-ray diffraction, photoluminescence, and UV-visible techniques were used as tools to monitor the degree of structural order in the PT:Sm system, being possible to identify the short- (disordered structure), intermediate- (intermediate structure), and long-range (crystalline structure) orders. Also investigated were the electronic structure and optical properties of PT:Sm using periodic *ab initio* quantum-mechanical calculations with the density functional theory (DFT). Thus, the influence of the doping element itself on the electronic configuration is just local; hence, it is not included in the simulation. The aim of the theoretical study is to investigate the electronic structure of PT:Sm using models representing its crystalline and disordered structures and give an interpretation in terms of the structure band, density of states (DOS), diagram levels, charge density lines, contours, and surface plots of the conditions allowing photoluminescence (PL) to occur at room temperature. This dual approach renders a plausible quantitative description of the behavior of PT:Sm under laser excitation and interesting correlation between the theoretical and experimental results.

II. EXPERIMENT

PT:Sm powders were prepared by the polymeric precursor method. Lead (II) acetate trihydrate $[Pb(CH_3COO)_2 \cdot 3H_2O]$, samarium oxide ($Sm_2O_3$), and titanium (IV) isopropoxide ($Ti[OCH(CH_3)_2]_4$) were used as starting materials. Ethylene glycol and citric acid were used as polymerization/complexation agents for the process. Ammonium hydroxide was used to adjust the *p*H and to prevent lead citrate precipitation.

Titanium citrate was formed by the dissolution of $Ti[OCH(CH_3)_2]_4$ in an aqueous solution of citric acid (60–70 °C). After the Ti-citrate solution was homogenized, a stoichiometric amount of $[Pb(CH_3COO)_2 \cdot 3H_2O]$ was dissolved in water and then added to the Ti-citrate solution, which was kept under slow stirring until a clear solution was obtained. In the preparation of the samarium solution, Sm_2O_3 was first dissolved in nitric acid and gradually added to the Pb–Ti-citrate solution.

Ammonium hydroxide was added until the *p*H reached 6–7. After homogenization of the solution containing the Pb^{2+}, Ti^{4+}, and Sm^{3+} cations, ethylene glycol was added. Upon continued heating at 80–90 °C, the solution became more viscous, forming a polymeric resin with no visible phase separation. The molar ratio of lead-samarium-titanium cations was 0.96:0.04:1, respectively, the citric acid/metal molar ratio was fixed at 3:1, and the citric acid/ethylene glycol mass ratio was fixed at 60:40.

The polymeric resin (gel phase) was heated at 250 °C for 3 h and at 300 °C for 1 h to promote the polymer pyrolysis process without crystallization. The polymeric precursor thus obtained was deagglomerated and heated at 300 °C for 16 h. The resulting material was heat treated at different temperatures for 2 h under an O_2 atmosphere.

The powders were analyzed by x-ray diffraction (XRD), using a Rigaku DMAX 2500 PC diffractometer in a θ-2θ configuration ranging from 5° to 75°, $\lambda = 1.5406$ Å, with a graphite monochromator. The Rietveld refinements[28] were carried out with the program GSAS.[29] The peak profile function was modeled using the convolution of the Thompson-Cox-Hastings pseudo-Voigt (pV-TCH) with the asymmetry function described by Finger *et al.*[30] The strain anisotropy broadening has been corrected by the phenomenological model described by Stephens.[31]

The photoluminescence spectra were measured using a U1000 Jobin-Yvon double monochromator coupled to a cooled GaAs photomultiplier and a conventional photon counting system. The 488.0 nm exciting wavelength of an argon-ion laser was used, with the laser maximum output power kept within 200 mW. The spectral dependence of the optical reflectance, UV-visible (UV-vis), of the PT:Sm was taken in the total reflection mode, using Cary 5G equipment. All the measurements were taken at room temperature.

TABLE I. Cell parameters (Å), tetragonal distortion c/a, volume ($Å^3$) and atomic fractional coordinates obtained by Rietveld refinement to Sm-doped PT. The R indexes are defined by Larson and Von Dreele.[29]

$a=b=3.9207$ Å,	$c=4.0684$ Å,	$c/a=1.0376$,	$V=62.551$ $Å^3$
Atoms	x	y	z
Pb	0.0	0.0	0.0
O1	0.5	0.5	0.1255
O2	0.5	0.5	0.5995
Ti	0.5	0.5	0.5276

$R_{wp}=9.88\%$, $R_F{}^2=3.38$, $R_F=1.84\%$, $S=1.281$

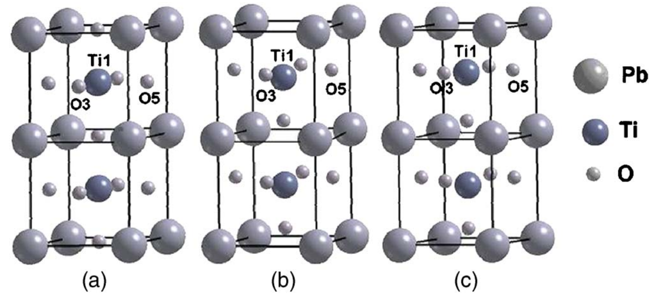

FIG. 1. Representation of the periodic model supercell $1\times1\times2$ of the (a) PT_{theor}, (b) PT:Sm_c, and (c) PT:Sm_d.

III. COMPUTATIONAL METHODS AND PERIODIC MODELS

The CRYSTAL98 program[32] was used to analyze the theoretical structure and the electronic properties of the Sm-doped PT. This method allowed us to perform band structure calculations with optimized structures of PT, either ordered (crystalline) or disordered. The calculations were carried out within the framework of DFT and performed with the B3LYP (gradient-corrected correlation functional) by Lee *et al.* combined with the Becke3[33,34] exchange functional. This computational technique has been used by Muscat *et al.*[35] to calculate structural parameters and band structures for a wide variety of solids.

This functional technique has already been successfully employed in studies of the electronic and structural properties of the bulk and surfaces of various compounds, in particular, $PbTiO_3$[36] and $Ba_{0.5}Sr_{0.5}TiO_3$[18] systems. In the $PbTiO_3$ system, the atomic centers Pb, Ti, and O have been described by basis set in the schemes [DB]-31G, 86411-d(41) and 6-31G*, respectively.[37] Here [DB] stands for the Durand-Barthelats nonrelativistic large effective core potential.[38] These basis sets can be found at the CRYSTAL homepage. For the atomic positions and lattice parameters the Rietveld refinement analysis from the PT x-ray diffraction data were used (Table I). Similarly, based on the work reported by De Lazaro *et al.*,[19] the disordered structure was represented by the displacement of the Ti atom of 0.2 Å. It should be stressed that such displacement leads to the occurrence of the Jahn-Teller effect in the displaced structure. The periodic models allowed us to obtain information on the general effects of the dopant on the electronic structure.

The behavior attributed to the difference in the electronic density of the Pb^{2+} and Sm^{3+} ions is directly related to the influence of the samarium content in the PT:Sm phase transition from a tetragonal to cubic one. This can be verified by the calculations of the tetragonality factor (c/a) presented on Table I. The c/a ratio was 1.052 and 1.038 for pure PT and PT:Sm, respectively. The decrease of the tetragonality factor with the samarium presence indicates that the material is approaching to cubic phase. This phase transition can be understood by considering the formation of Pb^{2+} vacancies when these ions are replaced by Sm^{3+}. These vacancies may relax the lattice, turning it more symmetrical.

PT crystallizes in two possible structures: cubic and tetragonal. An optimization of the cell parameters, based on the perfect atomic position, was used to create the cubic structure model designated by PT_{theor}. This cubic structure was compared with the crystalline tetragonal structure and with the disordered tetragonal structure. This third model represents the PT cubic structure as it should be at 0 K, i.e., with an ideal structure [Fig. 1(a)].

In this work, we focus on the tetragonal structure (space group $P4$ mm) following the experimental results [see Figs. 1(b) and 1(c)]. The cell and atomic position parameters used in the calculations are taken from results of Rietveld refinements (Table I). For both the Sm-doped experiment (PT:Sm_c) to simulate the crystalline structure with D_{4h} symmetry designated by $[TiO_6-TiO_6]$ and for the periodic model designated by PT:Sm_d to simulate the disordered structure. In this periodic model the Ti atom was displaced by 0.2 Å along the c axis, using the ATOMDISP option provided with the CRYSTAL program. In this case, we have two types of environments for the titanium atom; one square-base pyramid structure and another octahedral structure with C_{4v} symmetry. This periodic model was designated as $[TiO_5-TiO_6]$.[16] These periodic models were simulated to study the optical, structural, and electronic properties of the disordered state of PT and to understand the photoluminescence phenomenon of this material at room temperature.

IV. RESULTS AND DISCUSSION

Figure 2 shows the XRD patterns of the PT:Sm powders calcined at 370, 380, 390, 400, 405, 410, and 450 °C. The powders obtained from 370 to 405 °C displayed a pattern of a typical disordered material, presenting a wide band, centered at $2\theta=28.9°$, whereas the samples heat treated at 410 and 450 °C showed a pattern of crystalline material (ordered structure) corresponding to the PT tetragonal perovskite phase. All the samples, disordered and ordered, were studied by photoluminescence.

Figure 3 illustrates PL spectra recorded at room temperature for the seven powders treated from 370 to 450 °C in oxygen atmosphere. They were excited by the 488 nm line of an argon laser and emit in the visible part of the spectra. The bands are broad and intense, mostly for the disordered powders treated at 405 °C. These broad bands are typical of multiphonons process, i.e., a system in which relaxation occurs by various paths, involving the participation of numerous states. Also, it is considered that this visible emission

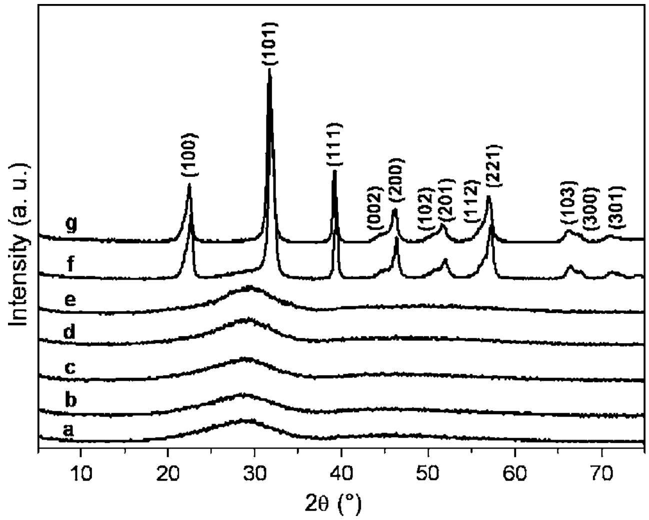

FIG. 2. X-ray patterns of the PT:Sm powders calcined at (a) 370, (b) 380, (c) 390, (d) 400, (e) 405, (f) 410, and (g) 450 °C.

may be attributed to a direct recombination of a conduction electron in the titanium site and hole in the oxygen valence band. However, the excitation line used (488 nm) has an energy much lower than the band gap energy (3.18 eV for bulk $PbTiO_3$)[36] so that this direct recombination is improbable. In contrast, the luminescence is intense for Sm^{3+} which the excitation spectra show the peaks corresponding to valence-to-conduction band edge (T=390–450 °C).

Two narrow bands corresponding to the Sm^{3+} photoluminescence are observed at 380 °C, indicating the beginning of the structural organization in the short range. This may be connected with the point symmetry at the Sm^{3+} site, considering the fact that the number of symmetry operations increases with increasing of the order. At first sight, the titanium ion in solution is chelated by the oxygen and almost regular $[TiO_6]$ clusters without constraints are therefore formed, surrounded by a random distribution of network modifier ions. A certain kind of short range organization already exists in this gel formation. Then, during the gel calcinations at 300 °C, the organic compounds are eliminated but the local order is maintained.[39] An XRD analysis of the material obtained at this temperature (Fig. 2) presents a completely disordered pattern, showing that the beginning of the structural organization in the short and intermediate range of the material could not be characterized by this technique. It thus became clear that the broad PT band is associated with the disordered structure, which is composed of a random mixture of $[TiO_5]$ and $[TiO_6]$ clusters, leading to the appearance of electron levels in the valence band region.[16]

The most characteristic signature of such order in short range is the first PL peak of the Sm^{3+} within of the random mixture of $[TiO_5]$ and $[TiO_6]$ (T=380 and 390 °C). These features correspond to large real space distances in the PT:Sm, and understanding their origin is a key to unravel details of intermediate range order. In the case of PT:Sm, PL has provided clear evidence for anomalously short $[TiO_5]$–$[TiO_6]$ distances in the structure (noncrystalline structures), associated with the crystalline structure.

The sample treated from 400 to 405 °C exhibited a third narrow band ascribed to Sm^{3+} in the PL spectrum, indicating the signature of short- and intermediate-range orders. The structural differences are correlated to differences in the crystallization behavior, possibly because the intermediate-order influences in the nucleation of the crystalline phase.[40] At 405 °C, an increase in the intensity of these narrow bands indicates the beginning of a long-range order.

The inset of Fig. 3 depicts the magnified PL spectra of the powders obtained at 410 and 450 °C. In this temperature range, the material presents a long-range periodic order. This can be clearly observed by XRD where the peaks of the PT:Sm crystalline phase are well defined. The powder heat treated at 410 °C exhibits a low intensity broad band

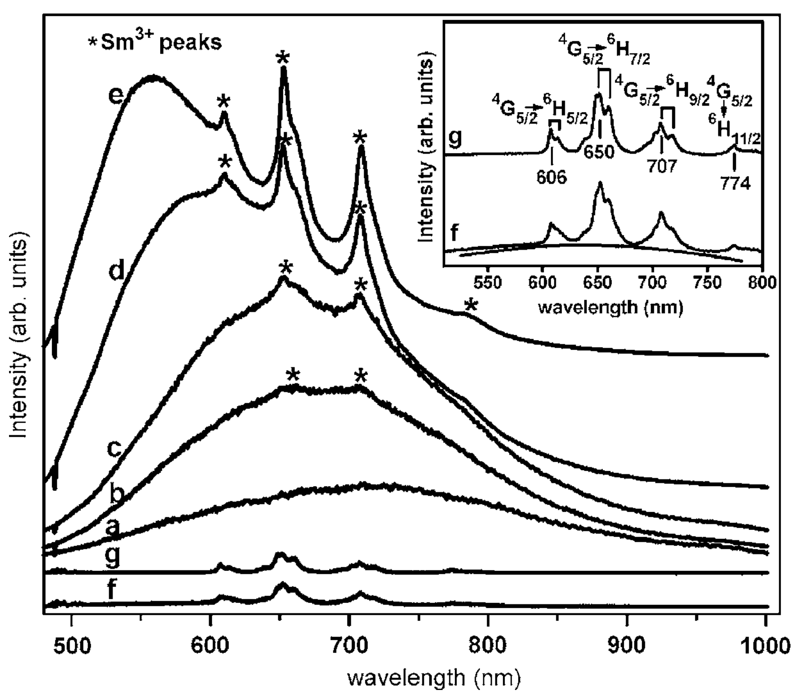

FIG. 3. PL spectra of the PT:Sm powders calcined at (a) 370, (b) 380, (c) 390, (d) 400, (e) 405, (f) 410, and (g) 450 °C.

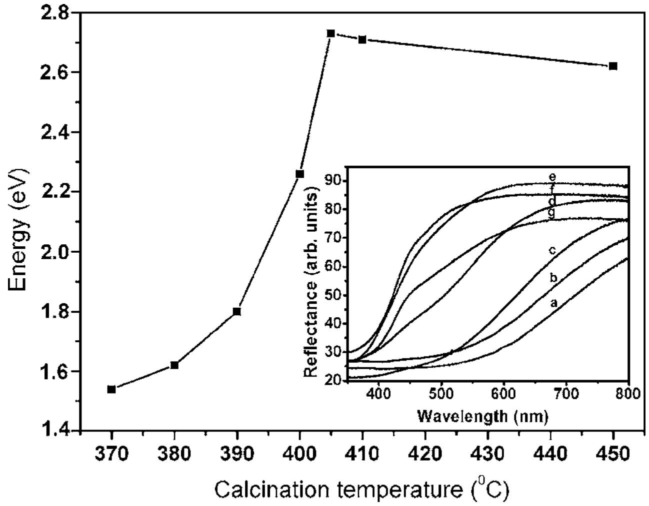

FIG. 4. Band gap energy variation as a function of the calcination temperature. The inset shows the spectral dependence of the reflectance for the PT:Sm powders obtained at (a) 370, (b) 380, (c) 390, (d) 400, (e) 405, (f) 410, and (g) 450 °C.

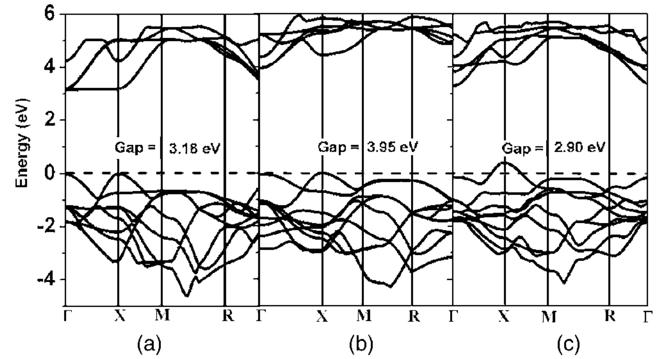

FIG. 5. Band structure and value indirect gap for (a) PT_{theor} (3.18 eV), (b) PT6:Sm_c (3.95 eV), and (c) PT:Sm_d (2.90 eV).

corresponding to the PT:Sm photoluminescence and at 450 °C (completely crystalline structure) only high intensity narrow bands are noticed, corresponding to Sm^{3+} emission transitions: ${}^4G_{5/2} \rightarrow {}^6H_{5/2}$ (606 nm), ${}^4G_{5/2} \rightarrow {}^6H_{7/2}$ (650 nm), ${}^4G_{5/2} \rightarrow {}^6H_{9/2}$ (707 nm), and ${}^4G_{5/2} \rightarrow {}^6H_{11/2}$ (774 nm). From the emission spectra measured at 450 °C (inset of Fig. 3), three emission transitions were found to be split into two components, according to Hussain *et al.*[27]

At 450 °C, the material presented a high structural order (only [TiO_6] clusters are present) and no PT:Sm photoluminescence is observed, since this effect depends on a certain degree of structural disorder in the material.

Figure 4 presents the evolution of the optical band gap, determined from the reflectance spectra following the Wood-Tauc method,[41] as a function of the calcination temperature. The lowest energy gap value refers to a highly disordered material (370 °C). This structural disorder generates a high number of defects which is responsible for the low energy gap. It is observed that the optical energy gap values increase with the long-range periodicity. However, for the powders calcined at temperatures higher than 405 °C the energy gap variation is not significant.

The inset of Fig. 4 exhibits the spectral dependence of the optical reflectance for the disordered, intermediate, and ordered states of the PT:Sm. In the case of the powders calcined at 370, 380, and 390 °C, the same features were observed. A different behavior is observed for the powder calcined at 400 °C, indicating a structural order, in agreement with the PL results. In the case of ordered PT:Sm (450 °C), the slope of the curve is higher than in the case of the structurally disordered samples.

This set of experiments shows that the displacement evidenced by photoluminescence in this simple perovskite compound should be essentially dynamic and result from the crossover from order-disorder to order regime, as a function of temperature.

The values of the measured optical gaps (Fig. 4) for the disordered and crystalline PT:Sm are, respectively, 2.60 eV at 450 °C and 1.80 eV at 380 °C. These results indicate that in this case the PL is directly related to the exponential optical absorption edge and the optical band gap is controlled by the structural disorder degree in the network of the PT:Sm sample. Observed was a decrease in the band gap that can be ascribed to defects or impurities, which induce the appearing of intermediary energy levels within the band gap, promoted by the structural disorder of the PT.[18]

The Rietveld refinements show that the presence of Sm induces slight variations in the cell parameter, thus leading to a small increase of the tetragonal distortion. The small increases of the tetragonal leads to the higher deformation of the [TiO_6] octahedra in Sm-doped PT. The samarium introduction increases the disorganization of the crystal.

Figures 5(a)–5(c) show the band structure to the PT_{theor}; PT:Sm_c, and PT:Sm_d, respectively. The calculated band structure shows for PT in the high-symmetry directions in the Brillouin zone in Fig. 5(a). The energy is in eV and the origin of energy was arbitrarily set to be at the maximum valence band. In these figures we find a large dispersion of the bands.

The gap value is determinated by the top of the valence band (VB) and is at the X point and the bottom of conduction band (CB) is at the Γ point. Between the points X and Γ was observed the minimum indirect gap with values of 3.18, 3.95, and 2.90 eV for the PT_{theo}, PR:Sm_c, and PT:Sm_d, respectively. A comparison among PT_{theor}, PT:Sm_c, and PT:Sm_d shows almost discernible difference.

These results are in agreement with the interpretation that the exponential optical absorption edge and the optical band gap are controlled by the disorder degree, structural, and controlled thermal effect.

The energy diagram levels for cubic PT_{theor} and tetragonal PT:Sm_c, and PT:Sm_d are presented in Figs. 6(a)–6(c), respectively. The VB is in the top of energy diagram levels and CB is in the bottom. The band gap is between VB and CB. In the analyzed energy diagram levels for the PT_{theor}, PT:Sm_c, and PT:Sm_d in the VB region are observed the contribution of oxygen atoms derived from the $2px$, $2py$, and $2pz$ atomic orbital. The contribution of the titanium atoms present in the CB region is the $3dxy$, $3dzy$, $3dzx$, $3dx^2-y^2$, and $3dz^2$ atomic orbital. We can observe in Fig. 6(a) that exist a gap of 3.18 eV from the transition-metal d-derived conduction band. These splittings are produced by the crystal

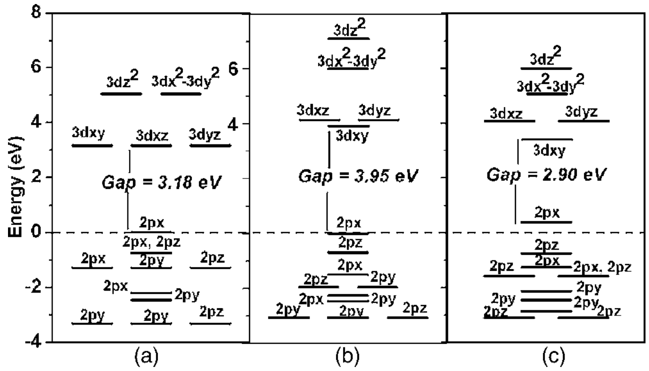

FIG. 6. Representation of diagram of levels for the (a) PT_{theor}, (b) $PT:Sm_c$, and (c) $PT:Sm_d$.

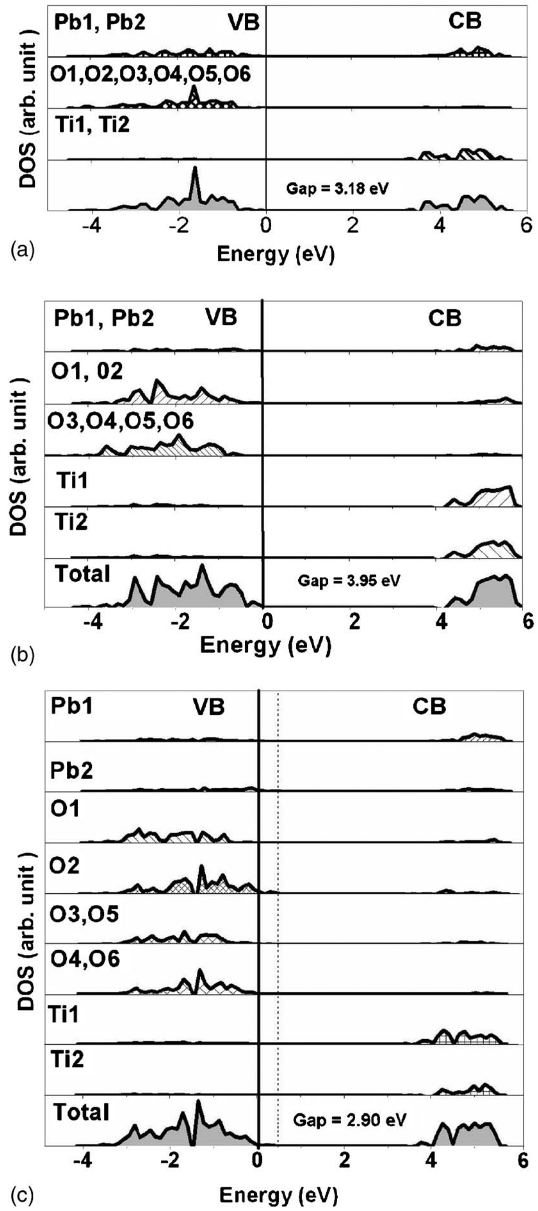

FIG. 7. Density of states (DOS) total and projected over the oxygen and titanium atoms to (a) PT_{theor}, (b) $PT:Sm_c$, and (c) $PT:Sm_d$.

field and the electrostatic interaction between oxygen $2p$ atomic orbitals. In the conduction band the triple and double degenerated levels represent t_{2g} and e_g states of titanium $3d$ orbital separated by energy of 1.88 eV. Figure 6(b) shows that top VB, the atomic orbital oxygen $2p$, is in 0 eV and the botton CB, the atomic orbital $3d$, the Ti atoms are in 3.95 eV. The orbital $3d$ of the Ti atoms presents a decrease in the degenerescencies of these atomic orbital. These results are coexistent with Jahn-Teller effect caused by displacement of Ti in $PT:Sm_d$ model.

Figure 6(c) shows that the top VB of the $PT:Sm_d$ in the energy diagram levels is constituted by the contribution of atomic orbital of the oxygen atoms and the symmetry breakage of formerly degenerate atomic orbital can be observed for the oxygen atoms, inducing energy levels appearing in the band gap region. From this fact a decrease in the band gap value results for the disordered structure. These results are consistent with the Jahn-Teller effect caused by the displacement of titanium (1) in $PT:Sm_d$ model.

The calculated total and atom-resolved partial DOS for the Pb, O, and Ti atoms, for the PT_{theor}, and tetragonal $PT:Sm_c$ and $PT:Sm_d$ periodic models are shown in Fig. 7(a)–7(c) respectively. For both the PT_{theor} and $PT:Sm_c$ the VB is observed between 0 and −4.52 eV and the CB between 3.18 and 5.72 eV and 3.95 and 6 eV, respectively. For the $PT:Sm_d$ VB is between 0.5 and −4.19 eV and CB is between 2.95 and 5.85 eV. The DOSs for both periodic models observed in the VB region are similar, and it can be observed that there is a predominant contribution of oxygen atoms derived from $2p$ atomic orbital. For the CB, the predominant contributions are due to titanium atoms derived from $3d$ atomic orbital. The decreasing of the gap values of the periodic model $PT:Sm_d$, brought about by the disorder, noticed from the DOS analysis, indicates that in the disordered material the oxygen $2p$ atomic orbital promotes the decrease in the band gap value, which is responsible for the photoluminescence phenomenon at room temperature in the visible range.

We built the diagram of charge density contour-surface plots for cubic PT_{theor} and tetragonal $PT:Sm_c$ and $PT:Sm_d$ in the horizontal plane passing by the Ti1, O3, and O5 [see Fig. 8 for (a) PT_{theor}, (b) $PT:Sm_c$, and (c) and (d) $PT:Sm_d$, respectively]. An analysis of Fig. 8 clearly shows that the bonding between Pb and $[TiO_6]$ is strongly ionic, while a covalent bonding nature is visible between Ti and O, result of the hybridization between the O ($2p$) states and the Ti ($3d$) states. The Ti–O bond is also strongly covalent. The breaking of the Ti1–O2 bond is visible in Fig. 8(c). The displacement of the Ti of 0.2 Å ongoing from $PT:Sm_c$ to $PT:Sm_d$ results in the deformation of a symmetric $[TiO_6–TiO_6]$ structure into two fragments: $[TiO_5]$ and $[TiO_6]$. The formal charge indicated in Figs. 8(a) and 8(b) shows the symmetric $[TiO_6]–[TiO_6]$ to cubic and tetragonal that possesses a quite regular charge repartition on both clusters, $-1.06e$ and $-0.96e$, respectively. In the case of the deformed structure, the formal charge of the $[TiO_5]$ and $[TiO_6]$ clusters become $-0.42e$ and $-1.49e$, respectively. A permanent charge gradient is thus created between $[TiO_6]$ and $[TiO_5]$ to compensate the breaking of Ti1–O2 bond [as defined in Fig. 8(c) and 8(d)]. The charge transfer occurs from one cluster to another and not from the oxygen atom to one

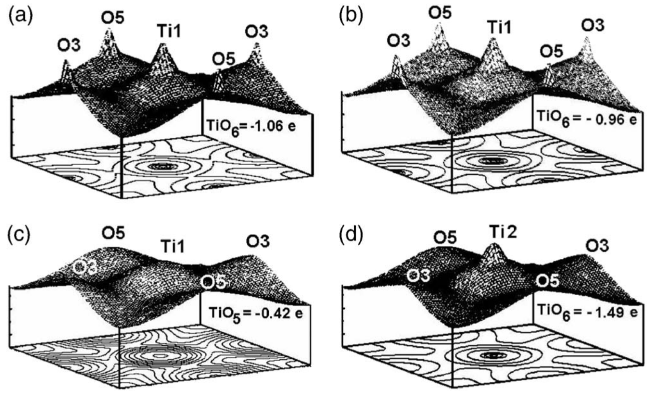

FIG. 8. Diagram the charge density contour-surface plots for (a) PT_{theor} (TiO_6=−1.06*e*), (b) PT:Sm_c (TiO_6=−0.96*e*), (c) PT:Sm_d (TiO_5=−0.42*e*), and (d) PT:Sm_d (TiO_6=−1.49*e*).

titanium atom, as widely seen in the literature.[7] This charge gradient and the presence of the localized states provide very good conditions for the trapping of electrons and holes, which radiative recombination is responsible for the PL of the disordered powders.

Nevertheless, the theoretical results obtained by the structure band, DOS, and diagram levels for such displacement pointout to meaningful differences in the region of band gap. For instance, the band gap energy decreased from 3.95 eV for the PT:Sm_c to 2.90 eV for the PT:Sm_d.

The differences between PT_{theor}, PT:Sm_c, and PT:Sm_d are well defined. The PT_{theor} model is the most ordered and Ti–O coordination is regular. The PT:Sm_c and PT:Sm_d models tend to cubic structure. These cubic tendencies are the result of the deformations existing in the structures and that are compensating the stress caused by the Pb. The atomic orbital titanium 3*d* and upper atomic orbital oxygen 2*p* are strongly perturbed by the disorder in the experimental structures and their splitting is not typical of the octahedral coordination like in PT_{theor} model. The splitting of the atomic orbital 3*d* of titanium atom is due to the effect of the octahedral crystal field of the six oxygens surrounding the titanium. In the PT:Sm_c model, the titanium 3*d* states are perturbated because of the Ti–O bond distances, angles, and dihedral angles are not regular anymore. This modification in the splitting of the 3*d* orbital can be associated with the Jahn-Teller effect, that not only breaks the local point symmetry but simultaneously also the translational symmetry.

The formation of fivefold oxygen-titanium coordination $[TiO_5]$ is caused by the displacement of the titanium atom (Ti1). Thus, the Ti1–O2 bond introduces localized electronic levels of the oxygen atom (O2) atomic orbital $(2px, 2py, 2pz)$ in the band gap region, decreasing its value. The experimental results of the UV-vis spectra and the corresponding optical band gaps obtained by the Wood-Tauc method,[41] as well as the PL measurements, agree with the theoretical results and are consistent with the expected Jahn-Teller[42] effect caused by the displacement of Ti1 in PT:Sm_d model. According to Korzhik *et al.*[43] and Kan *et al.*[44] hypotheses, we assumed the formation of vacant localized states linked to local defects like oxygen vacancies in the band gap above the valence band and below the conduction band. In the model presented by Leonelli and Brebner,[45] some of the electrons were promoted to the conduction band by absorption of photon forming small polarons. The polaron interacts with holes trapped in the crystal (defects or impurities) and form self-trapped excitons (STE).[7] In our model, the most important events occur before excitation. The structural and intermediate defects of localized states in the band gap and inhomogeneous charge distribution in the disordered system allow the trapping of electrons.

V. CONCLUSION

In summary, the polymeric precursor method was shown to be efficient in the preparation of Sm-doped $PbTiO_3$ and XRD, PL, and UV-vis techniques were good tools in the characterization of the structural order-disorder transformations, promoted by a controlled heat treatment. Due to the characteristic signature of the Sm^{3+} within of the random mixture of $[TiO_5]$ and $[TiO_6]$, this ion was efficient as marker of the short-, intermediate-, and long-range orders using PL technique. A periodic *ab initio* quantum-mechanical study was undertaken and allow to describe two main factors that are responsible for the PL of the PT:Sm_d: (a) the appearance of electronic levels in region of band gap and (b) the coexistent of both $[TiO_6]$ and $[TiO_5]$ cluster configurations in PT:Sm_d, due to the displacement of the titanium atom (Ti1). The periodic disordered model will generate localized states that allow the trapping of the holes and the electrons at lower energies, and thus a radioactive recombination. Moreover, 1*e* charge transfer occurs from the $[TiO_5]$ cluster to the $[TiO_6]$ one, revealing the intrinsic presence of trapped holes and electrons before the excitation. It is important to stress that computational chemistry has efficiently explained the results of experimental investigation, and the work presented here demonstrates that the joint use of theory and experiment represents a unique opportunity for investigating PL properties in perovskite materials.

ACKNOWLEDGMENTS

The authors acknowledge the Brazilian financing agencies FAPESP/CEPID, CNPq/PRONEX, CAPES, and CNPq/FAPESQ/PRODOC.

[1] J. Ballato, R. Esmacher, R. Schwartz, and M. Dejneka, J. Lumin. **86**, 101 (2000).
[2] H. Liu, S. T. Li, G. K. Liu, W. Jia, and F. E. Fernandez, J. Lumin. **83**, 367 (1999).
[3] V. Trapakov, V. Dimza, L. Jastrabik, A. Savinov, and Z. Bryknar, Phys. Status Solidi B **183**, 299 (1994).
[4] Z. Bryknar, V. Trepakov, Z. Potucek, and L. Jastrabik, J. Lumin. **87**, 605 (2000).
[5] S. Murakami, M. Morita, M. Herren, T. Sakurai, and D. Rau, J. Lumin. **87**, 694 (2000).
[6] W. F. Zhang, Z. Yin, and M. S. Zhang, Appl. Phys. A: Mater. Sci. Process. **70**, 93 (2000).
[7] J. Meng, Y. Huang, W. Zhang, Z. Du, Z. Zhu, and G. Zou, Phys. Lett. A **205**, 72 (1995).
[8] B. Bouma and G. Blasse, J. Phys. Chem. Solids **56**, 261 (1995).
[9] S. Myhajlenko *et al.*, J. Appl. Phys. **97**, 014101 (2005).
[10] T. L. Chen, X. M. Li, K. S. Wan, W. L. Zhu, and G. Pezzotti, Appl. Phys. Lett. **87**, 181914 (2005).
[11] Y. H. Lin, C. W. Nan, J. F. Wang, H. C. He, J. Y. Zhai, and L. Jiang, Mater. Lett. **58**, 829 (2004).

[12]T. Hara, Solid State Commun. **132**, 109 (2004).
[13]Z. X. Chen, Y. Chen, and Y. S. Jiang, J. Phys. Chem. B **105**, 5766 (2001).
[14]Z. X. Chen, C. G. Liu, Y. Chen, and Y. S. Jiang, Chem. Phys. **270**, 253 (2001).
[15]J. Goniakowski, J. M. Holender, L. N. Kantorovich, M. J. Gillan, and J. A. White, Phys. Rev. B **53**, 957 (1996).
[16]P. S. Pizani *et al.*, Appl. Phys. Lett. **77**, 824 (2000).
[17]E. Orhan *et al.*, Phys. Rev. B **71**, 085113 (2005).
[18]E. Longo *et al.*, Phys. Rev. B **69**, 125115 (2004).
[19]S. R. De Lazaro, E. R. Leite, E. Longo, and A. Beltrán, Bol. Soc. Esp. Ceram. Vidrio **43**, 644 (2004).
[20]Y. Zhang *et al.*, Nucl. Instrum. Methods Phys. Res. B **218**, 89 (2004).
[21]C. A. Kodaira, H. F. Brito, E. E. S. Teotonio, M. Claudia, M. C. F. C. Felinto, O. L. Malta, and G. E. S. Brito, J. Braz. Chem. Soc. **15**, 890 (2004).
[22]S. Singh, O. P. Thakur, C. Prakash, and K. K. Raina, Physica B **355**, 280 (2005).
[23]S. Singh, O. P. Thakur, and C. Prakash, J. Phys. D **38**, 1621 (2005).
[24]A. Polman, J. Appl. Phys. **82**, 1 (1997).
[25]A. Patra, Chem. Phys. Lett. **387**, 35 (2004).
[26]H. Liang, Y. Tao, Q. Su, and S. Wangw, J. Solid State Chem. **167**, 435 (2002).
[27]N. S. Hussain, V. Aruna, and S. Buddhudu, Mater. Res. Bull. **35**, 703 (2000).
[28]H. M. Rietveld, J. Appl. Crystallogr. **2**, 65 (1969).
[29]A. C. Larson and R. B. Von Dreele, Los Alamos National Laboratory Report No. LAUR 86-748, 2004 (unpublished).
[30]L. W. Finger, D. E. Cox, and A. P. Jephcoat, J. Appl. Crystallogr. **27**, 892 (1994).
[31]P. W. Stephens, J. Appl. Crystallogr. **32**, 281 (1993).
[32]R. Dovesi, V. R. Saunders, C. Roetti, M. Causà, N. M. Harrison, R. Orlando, and E. Aprà, *CRYSTAL 98 User's Manual* (University of Torino, Torino, 1998).
[33]C. Lee, W. Yang, and R. G. Parr, Phys. Rev. B **37**, 785 (1988).
[34]A. D. J. Becke, Chem. Phys. **98**, 5648 (1993).
[35]J. Muscat, A. Wander, and N. M. Harrison, Chem. Phys. Lett. **42**, 397 (2001).
[36]S. de Lazaro, E. Longo, J. R. Sambrano, and A. Beltran, Surf. Sci. **552**, 149 (2004).
[37]http://www.chimifm.unito.it/teorica/crystal/crystal.html
[38]P. Durand and J. C. Barthelat, Theor. Chim. Acta **38**, 283 (1975).
[39]F. M. Pontes *et al.*, Mater. Chem. Phys. **78**, 227 (2003).
[40]T. C. Hufnagel, Nat. Mater. **3**, 666 (2004).
[41]D. L. Wood and J. Tauc, Phys. Rev. B **5**, 3144 (1972).
[42]S. Lenjer, O. F. Schirmer, H. Hesse, and T. W. Koll, Phys. Rev. B **66**, 165106 (2002).
[43]M. V. Korzhik, V. B. Pavlenko, V. A. Lium, I. M. Solskii, and J. P. Peigneux, Phys. Status Solidi A **154**, 779 (1996).
[44]D. Kan *et al.*, Nat. Mater. **4**, 816 (2005).
[45]R. Leonelli and J. L. Brebner, Phys. Rev. B **33**, 8649 (1986).